

# Molecular Dynamics Study of Palladium Clusters: Size Dependent Analysis of Structural Stabilities and Energetics of Pd<sub>n</sub> ( $n \leq 40$ ) via a Lennard-Jones Type Potential

Mustafa Büyükatana,\* and Jadson C. Belchior<sup>b</sup>

<sup>a</sup>Department of Physics, Bozok University, 66200, Yozgat, Turkey

<sup>b</sup>Departamento de Química – ICEx, Universidade Federal de Minas Gerais, Pampulha, (31.270-901)  
Belo Horizonte, MG, Brazil

RECEIVED AUGUST 14, 2007; REVISED FEBRUARY 22, 2008; ACCEPTED FEBRUARY 29, 2008

*Keywords*  
cluster  
palladium  
Lennard-Jones type potentials  
Molecular Dynamics

Possible stable structures and energetics of palladium clusters, Pd<sub>n</sub> ( $n = 2-40$ ), have been investigated by performing molecular-dynamics simulations based on a Lennard-Jones type pair-potential. To determine a preferable growth mechanism, the growing pattern of Pd<sub>n</sub> clusters was analyzed via rearrangement collisions and the simple quenching technique. Main observed results are that palladium clusters prefer three-dimensional structures and spherical clusters of medium size appear to have five-fold symmetry. The results are compared with those from previous theoretical studies.

## INTRODUCTION

In the area of nano-science, considerable research has been widely carried out on atomic and molecular clusters.<sup>1-6</sup> Understanding of the physical and chemical properties of bulk matter through finite nano-scale aggregates is one of the motivations for these researches.<sup>5</sup> Therefore various properties of clusters have been studied such as their interactions with molecules,<sup>6,7</sup> melting, isomerisation<sup>8,9</sup> and chaotic behaviors.<sup>10</sup> Although the medium-size clusters look simple and show some bulk features, their geometrical and electronic structures are not well-determined.<sup>11-15</sup> Particularly, investigations on small clusters have revealed their strong size dependent properties, which can be attributed to changes in geometrical structures as the number of atoms increases.

Transition-metal (TM) nano-systems have been extensively studied from the cluster point of view for a relatively long time because of their scientific and technological interests.<sup>16-22</sup> Experimental results of TM clusters have indicated the distinction of complexity in both geometrical structure and magnetism.<sup>8-10,23-26</sup> The experimental detection of the exact geometric structure of clusters is still a hard task. Structures and cohesive energies of clusters can not be obtained directly from gas phase or molecular beam experiments. Hence, theoretical investigations play an important role in cluster studies. It is possible to make effective theoretical predictions using density functional theory (DFT)<sup>27</sup> for some unknown structures based on experimental measurements.<sup>25</sup> Despite of numerous simulations on atomic clusters there are still needs to study metallic clusters and there are

\* Author to whom correspondence should be addressed. (E-mail: mustafa.boyukata@bozok.edu.tr)

many currently under investigation.<sup>28–30</sup> The geometries, especially for the energetically most favorable isomers of each size, are often crucial for comparisons which is a good knowledge of the potential energy surface (PES), a demanding task for computational analysis. In addition, the determination of magic numbers of clusters is required because the intensity of relatively stable clusters grows at the expense of their less stable ones.

In the present work, stable structures and magic numbers for Pd<sub>2</sub>–Pd<sub>40</sub> clusters are reported. There are various interesting theoretical and experimental studies in the literature on palladium clusters. For example, high resolution electron microscopy study shows that small Pd particles are icosahedral.<sup>31</sup> Josè-Yacamen *et al.*,<sup>32</sup> reported cuboctahedral, twinned decahedral and amorphous structures for nano-scale particles. In general, the tendency for fcc structures is expected to be high for larger Pd clusters. A tendency for pentagonal symmetry structures and twin formation for dispersed Pd deposits on different supports have been reported.<sup>33</sup> Theoretical calculations using molecular orbital and DFT methods have been reported for small Pd clusters.<sup>34–36</sup> Some computations have been performed on Pd clusters using empirical potentials.<sup>23,24,37,38</sup> Structures, energetics and isomers of Pd<sub>2</sub>–Pd<sub>20</sub><sup>23</sup> and Pd<sub>21</sub>–Pd<sub>55</sub><sup>24</sup> have been studied using Molecular Dynamics (MD) method and the Embedded Atom Model (EAM). Recently, H. Arslan<sup>28</sup> carried out a Monte Carlo (MC) simulation for Pd<sub>5</sub>–Pd<sub>80</sub> clusters using Sutton-Chen (SC) many-body potential. He has reported a detailed analysis of structures and energetics *via* the basin-hopping approach. Icosahedral, decahedral and fcc closed packed geometries were observed for Pd clusters.<sup>28</sup>

Here we have applied a simple quenching technique (to minimize the kinetic energy) on the rearranged systems after atom-cluster collisions in fusion regime,<sup>39</sup> for finding the low-energy structures of Pd clusters. The growth pattern of these clusters has been simulated using MD *via* a Lennard-Jones (LJ) type pair potential. Mohri *et al.*<sup>40</sup> modeled and parameterized this empirical potential for describing pair interaction energy of Fe-Fe, Pd-Pd and Fe-Pd nearest neighbor pairs in crystal systems. In a recent work,<sup>41</sup> we studied iron clusters with this potential function. In this particular calculation, we tested the potential for describing palladium clusters by a qualitative analysis and this potential can be used to describe structural growing sequences. The aim, among the structure and energetic analysis, was also to investigate the growing mechanism through the available empirical potential energy function for describing palladium system.

The paper is organized as follows. In section *Theoretical Background and Computational Methodology*, the classical MD method, used potential and the computational procedure are presented. In section *Results and Discussions*, the analysis of the findings are provided. Finally, the remarkable conclusions are given in section *Concluding Remarks*.

## THEORETICAL BACKGROUND AND COMPUTATIONAL METHODOLOGY

A classical MD method was applied for studying the Pd+Pd<sub>*n*-1</sub> collision system for formation of Pd<sub>2</sub>–Pd<sub>40</sub> clusters. The Hamiltonian to solve the classical Hamilton's equations generating the motions of the system is as follows:

$$H = \sum_{i=1}^n \frac{P_i^2}{2m_i} + \sum_{i<j}^n V(r_{ij}) \quad (1)$$

where the first term corresponds to the kinetic energy of the cluster,  $P$  and  $m$  are the moment and the mass of the atoms. The second term is the total potential energy of the whole  $n$ -particle system, a sum of all two-body interactions over the total pair interactions. The interactions between all particles in the system are described *via* a LJ-type pairwise potential.<sup>40</sup> The present analysis does not depend on the detailed form of the potential. This LJ type potential (hereafter LJ potential) is written according to

$$V(r_{ij}) = \varepsilon \left[ \left( \frac{\sigma}{r_{ij}} \right)^m - \frac{m}{n} \cdot \left( \frac{\sigma}{r_{ij}} \right)^n \right] \quad (2)$$

for a pair of atoms ( $i$  and  $j$ ) separated with distance  $r_{ij}$ . The used parameters are  $\sigma = 2.744 \text{ \AA}$  and  $\varepsilon = 15.0 \text{ kcal mol}^{-1}$ , respectively for atom-atom interaction.<sup>40</sup> These parameters were determined by fitting the experimental data of cohesive energies<sup>42,43</sup> and lattice constants of Pd.<sup>44</sup> The proposed values for  $m$  and  $n$  are 7.0 and 3.5, respectively.<sup>40</sup> Derivation of the potential for Pd-Pd nearest neighbor pairs is presented in Ref. 40 (for detail see Ref. 40 and related references therein).

Some of the main points of the computational procedure performed in this work will be described briefly. The initial potential energy of the system corresponds to the energy of the target Pd<sub>*n*-1</sub> cluster. Formation of the new cluster is related to the translation (collision/kinetic) energy of the new projectile atom. The potential has the new energy value depending on the final configuration of the new structure. The translation energy should be small enough to keep all particles of the system within the potential well; otherwise, the new  $n$ -atom cluster formation may not be possible. Occurrence of any fusion regime through an atom-cluster collision is very sensitive to collision energy<sup>39,41,45</sup> and the orientation of the clusters to produce the stable structures of resulting Pd<sub>*n*</sub> clusters. When the colliding atom hits the target cluster on any open site, a new structure is especially easily constructed. Hamilton's equations of motion have been solved by using the 5<sup>th</sup> and 6<sup>th</sup> order Runge-Kutta algorithm in the numerical integration. Cartesian coordinates are used in the trajectory space for time dependent positions and moments of the particles. The accuracies of the phase space coordinates and the conservation of energy (within the order of 10<sup>-10</sup>) are considered in step size

control of the micro canonical simulations. The collision energy of the projectile atom is distributed amongst the kinetic energies of all particles and the interaction occurs around the center of mass of the system during the simulation time,  $3.0 \times 10^6$  step. This run time interval is repeated for 5 different orientations of initial configuration. The  $\text{Pd}_n$  cluster is constructed through the atom-cluster collision in the fusion regime. All collisions are realized with low collision energies to avoid fragmentation and scattering. The orientation of the target clusters is randomly represented for reducing the site effects. Upon relaxation, the cluster rearranges substantially and the most stable one is determined through following each trajectory set by checking the potential energy of the system at 200 steps. The newly generated five configurations from each trajectory set are minimized by removing kinetic energy after  $5 \times 10^4$  relaxation steps and the corresponding structures are determined. The most stable one is determined through following each trajectory set by checking the potential energy of the system. Finally, the total energy ( $E$ ) becomes equal to the whole potential energy of the system,

$$E = \sum_{\substack{i=1 \\ j>i}}^n V(r_{ij}). \quad (3)$$

After determining the new  $\text{Pd}_n$  cluster, it is used for new collisions and these procedures are repeated to find new larger  $\text{Pd}_{n+1}$  clusters.

## RESULTS AND DISCUSSIONS

In this section the optimized structures of  $\text{Pd}_n$  ( $n = 2-40$ ) clusters, their growing path and magic behaviors are discussed. Figure 1 illustrates the obtained stable geometries of palladium microclusters up to 22-atoms. The  $\text{Pd}_2$ ,  $\text{Pd}_3$  and  $\text{Pd}_4$  clusters are small enough to allow possible minima to be directly constructed. The most stable geometry of  $\text{Pd}_4$  is a regular tetrahedron with  $T_d$  symmetry. The calculated values of bond length and binding energy for  $\text{Pd}_4$  are 2.74 Å and 0.98 eV/atom, respectively. In this approach a trigonal, an octahedron and a pentagonal bipyramids are predicted as ground state structures for  $\text{Pd}_5$ ,  $\text{Pd}_6$  and  $\text{Pd}_7$  clusters with 1.21, 1.47 and 1.65 eV/atom binding energies, respectively. The well-known ground-state structure of 7-atom cluster,  $\text{Pd}_7$  is also a pentagonal bipyramid of  $D_{5h}$  symmetry. In this work, the minimum displacements of pairs of atoms in these microstructures are 2.71, 2.70 and 2.68 Å. This value for the eight-atom palladium cluster is 2.67 Å. The determined stable structure of  $\text{Pd}_8$  is bidisphenoid with 1.81 eV/atom binding energy. In this building-up procedure for 9- to 12-atom clusters, the ground state geometries are in a growing pattern based on icosahedrons packing through filling of triangular open sites of the pentagonal bipyramid structures of  $\text{Pd}_7$ . The second pentagonal ring

is firstly observed in  $\text{Pd}_{12}$ . A Five-fold ring is a common backbone leading to a nearly perfect icosahedral form of  $\text{Pd}_{13}$ . In the particular case of  $\text{Pd}_{13}$ , the icosahedral configuration, a well-known magic structure, is predicted. The results up to 14 atoms are in good agreement with previously reported geometries of LJ clusters.<sup>46</sup> The binding energies for up to 13-atom Pd micro clusters are compared with previous studies<sup>23,28,47</sup> in Table I. The lowest energy value for  $\text{Pd}_{13}$  has been obtained with MC-SC.<sup>28</sup> The highest one has been calculated with an empirical PEF, Erkoç Potential (EP).<sup>47</sup> The binding energies ( $E_b$ ), the average interaction energy per atom in the cluster, were calculated using the computed total energy values ( $E$ ) as follow:

$$E_b = \frac{E}{n}. \quad (4)$$

We obtained a nonicosahedral symmetry ( $D_{6h}$ ) for  $\text{Pd}_{15}$  (Figure 1). It has a similar structural behavior like  $\text{Pd}_{13}$  cluster. Both of these are in closed cage structures each with an atom at the center. The ground state structures for  $\text{Pd}_{16}$ ,  $\text{Pd}_{17}$ ,  $\text{Pd}_{18}$  and  $\text{Pd}_{19}$  clusters were grown from the  $\text{Pd}_{13}$  geometry. The double icosahedral structure ( $D_{5h}$ ) is also found for  $\text{Pd}_{19}$ , another well-known magic size, in agreement with other studies.<sup>41,45</sup> From  $\text{Pd}_{20}$ , clusters atoms prefer to fill favorable hollow sites on the equatorial region of the double icosahedral form of  $\text{Pd}_{19}$ . There are 5 hollow sites on the equatorial ring of the  $\text{Pd}_{19}$  structure. A similar behavior was also observed for iron<sup>41</sup> and gold clusters in Refs. 41, 48 and 49. An atom collision with  $\text{Pd}_{20}$  produces a new  $\text{Pd}_{21}$  geometry by filling another hollow site. After this collision  $\text{Pd}_{21}$ , clusters reaches new more reactive sites, as common neighbors of these equatorial atoms. Due to their low coordination  $\text{Pd}_{22}$  prefers to grow from that site of  $\text{Pd}_{21}$ .

As the cluster size increases further, it becomes increasingly difficult to visualize the growth pattern. Even

TABLE I. The binding energies for  $\text{Pd}_n$  ( $n \leq 13$ ) micro clusters

$n$	MD-EAM <sup>23</sup>	MC-SC <sup>28</sup>	MD-EP <sup>47</sup>	This work
2	-0.35			-0.33
3	-0.79		-0.68	-0.65
4	-1.20		-0.95	-0.98
5	-1.46	-2.57	-1.10	-1.21
6	-1.71	-2.69	-1.22	-1.47
7	-1.86	-2.77	-1.32	-1.65
8	-1.97	-2.80	-1.33	-1.81
9	-2.06	-2.86	-1.32	-1.96
10	-2.15	-2.90	-1.43	-2.12
11	-2.22	-2.93	-1.49	-2.26
12	-2.32	-2.97	-1.55	-2.45
13	-2.45	-3.03	-1.63	-2.65

though the structural evolution of clusters is more complicated, it is possible to analyze the cluster formation mechanism. These structures are often based on the double icosahedral geometry with the additional atoms attached to various positions in the Pd<sub>19</sub> cluster. For microstructures consisting of a few atoms, it is easier to get a new structure by binding over a favorable open site. However, the new geometry for larger clusters may occur as local isomers of the new configuration due to their dislocated structures and high symmetries. In addition, from rearrangement structures it takes long computational time to obtain the stable geometry of the clusters unless the colliding atom hits the target at a suitable site. Therefore, the target position was randomly changed.

As shown in Figure 2, following this growing pattern, Pd<sub>23</sub> and Pd<sub>24</sub> are produced after adding atoms on the empty site on the equatorial ring. At the same time, two new and more reactive sites are produced on the surface. By filling these sites Pd<sub>26</sub> is constructed. Pd<sub>26</sub> has an interesting view of crossed shape of 19-atom geometry. As the consequence of this pattern, filling the empty and more reactive sites, all low coordination points on the equatorial region of Pd<sub>19</sub> are covered, one by one, on addition of atoms and finally a closed shell structure of Pd<sub>34</sub> is formed with 3 new five-atom rings. The structure

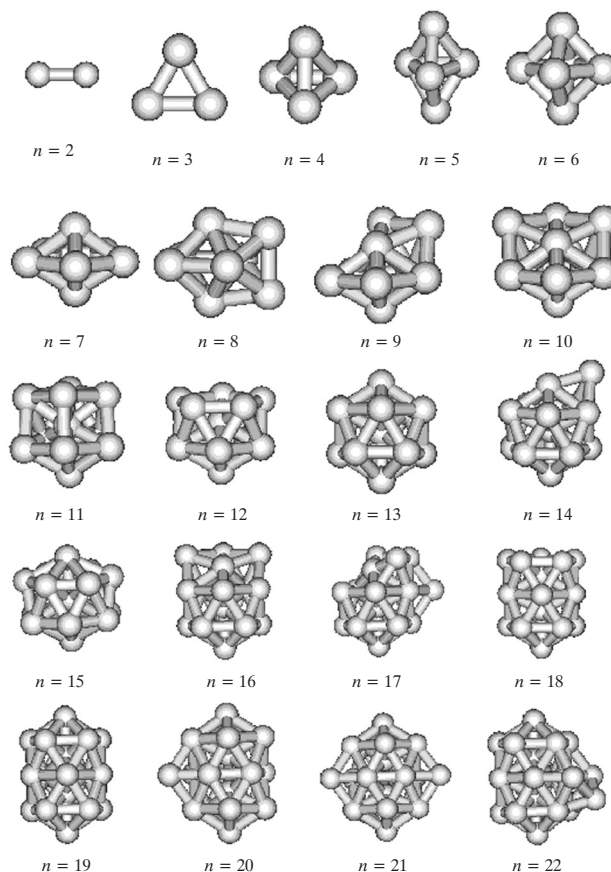


Figure 1. Optimized geometries for Pd<sub>2</sub>–Pd<sub>22</sub> clusters.

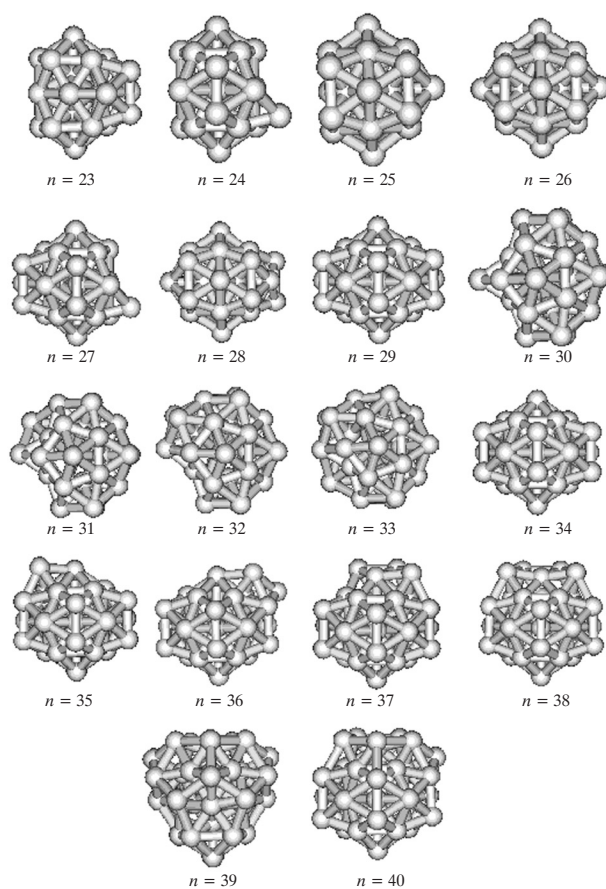


Figure 2. Optimized geometries for Pd<sub>23</sub>–Pd<sub>40</sub> clusters.

ral evolutions up to 40-atom clusters in this formation pattern are in the form of placing atoms on more reactive hollow sites of the Pd<sub>34</sub> geometry. As a result, the new larger size will continue to develop by filling the surface of the Pd<sub>34</sub> cluster. Increasing the number of atoms on the surface of the cluster leads to some structural distortions of the basic building elements. In most cases, the new optimized structure grew from hollow site of the previous smaller cluster. All configurations led to the migration of the colliding atom from the on-top or bridge site to an empty site because it is the most favorable adsorption site. The adsorbing atoms were generally introduced onto low coordinate Pd atoms due to reactivity of these atoms.

After finding the geometries up to Pd<sub>40</sub>, the magic behavior of these clusters was investigated. The binding energies versus the cluster size are plotted for the putative stable structures in Figure 3a. As the cluster size increases the average binding energy per atom decreases. This exponential-like decay is known as a common behavior almost for all metal clusters.<sup>45,50</sup> A central issue in cluster physics is to identify particularly stable sizes. A detailed structural picture and the nonmonotonic variation in the properties of clusters can be obtained by lo-

cating the global minimum as a function of size. This can then give information about abundances of particularly stable clusters.<sup>51</sup> The average binding energy per atom in the cluster may be, therefore, expressed as a function of the cluster size,<sup>52–54</sup>

$$E_{\text{fit}} = E_v + E_s n^{-1/3} + E_c n^{-2/3} + E_e n^{-3/3} \quad (5)$$

where the coefficients  $E_v$ ,  $E_s$ , and  $E_c$  correspond to the volume, surface, and curvature energies of the particles forming the cluster, respectively, and  $E_e$  defines the energy origin.<sup>55</sup> The fitted values of the coefficients are  $-13.919$ ,  $46.346$ ,  $-56.968$  and  $25.428$  eV/atom, respectively. The differences ( $E_b - E_{\text{fit}}$ ) between the binding energies of Equations (4) and (5) are plotted in Figure 3b. Fi-

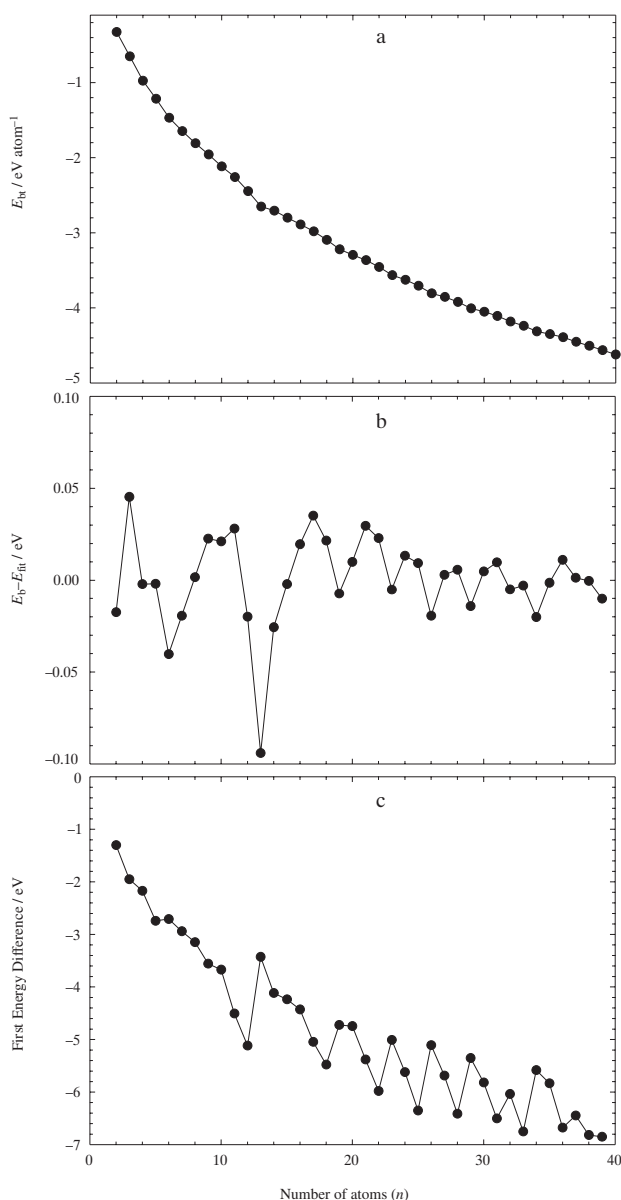


Figure 3. a) Binding energies, b)  $E_b - E_{\text{fit}}$  and c) First difference of the total energy for the obtained clusters up to Pd<sub>40</sub>.

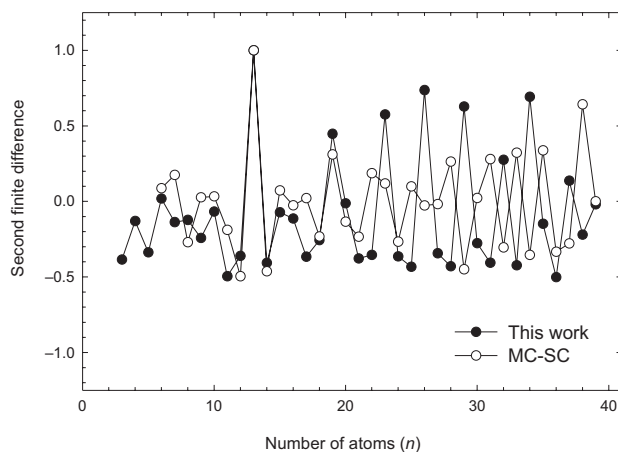


Figure 4. Second finite difference of the total energy for the obtained clusters up to Pd<sub>40</sub> (normalized with respect to the values of Pd<sub>13</sub>).

gure 3c illustrates the first energy difference of the total energy of the obtained clusters which is

$$\Delta_1 E = E_{n+1} - E_n \quad (6)$$

The second finite differences (the stability function) of the total energy of the determined clusters are calculated using the following equation:

$$\Delta_2 E = E_{n+1} + E_{n-1} - 2E_n \quad (7)$$

The values in Figure 4 are normalized with the value of Pd<sub>13</sub>. Through the peaks of these values, several exceptional stable structures are identified. These energetically most stable sizes are so-called magic clusters. Pd<sub>13</sub> is the first and the most stable magic cluster. Another well-known magic cluster like 13 atom size is Pd<sub>19</sub>. In this region, an interesting structure for palladium, Pd<sub>15</sub> also has a spherical geometry. However, it is not energetically more stable in spite of its close shell structure. Additionally, it was determined that 23, 26, 29, 32, 34 and 37 atom clusters also have magic behavior. Our calculation predicts that 34-atom palladium geometry has a close shell structure similar to the geometries of Pd<sub>13</sub>, Pd<sub>15</sub> and Pd<sub>19</sub>.

In order to understand more clearly the behavior of growing pattern and to be sure about the magic structure, we made displacement analysis of the atomic correlations. The atomic distances from the center of mass of the cluster and the pair displacements between atoms can demonstrate the close packing in the growing process. Figure 5 illustrates the displacements of atoms in the optimized structures for Pd<sub>2</sub>–Pd<sub>40</sub> clusters as a function of number of atoms ( $n$ ) in the clusters. The radial distribution is the distance of each atom with respect to the center of mass of a Pd <sub>$n$</sub>  cluster and it is given by

$$r_i = |R_i - R_0|, \quad R_0 = \frac{1}{n} \sum_{i=1}^n R_i \quad (8)$$

in which  $R_i$  is the position of the  $i^{\text{th}}$  atom. The radial distributions of atoms from the center of mass of the clusters are shown in Figure 5a. A maximum distance from the center provides information about the radius of cluster. The minimum distance of an atom from the center of mass of the cluster is the shifted position of the central atom, that is, the position of the closest atom to the center of mass. As expected the mean displacements from the center of mass of the clusters increase slightly due to the close packing phenomena. The maxima in the distances correspond to the more reactive sizes. Pd<sub>14</sub>, for example, has more reactive sites due to the low coordination. Especially the trends of the radii (maximum distances in the graph) have lower values identifying obviously for determined magic sizes. The microclusters up to 13-atoms grow *via* pushing an atom to the center. Pd<sub>4</sub> and Pd<sub>6</sub> have similar behavior because they have regular tetrahedral and octahedral structures, respectively. That is, all atoms have the same distance from the center. The first largest empty space is in the 6-atom microcluster and the second is verified in Pd<sub>8</sub>. Pd<sub>13</sub> and Pd<sub>15</sub> have an atom at their centers and the other atoms are surrounding this atom. Adding an atom to the spherical Pd<sub>13</sub> cluster causes to move the central atom away from the center in Pd<sub>14</sub>. After Pd<sub>15</sub>, the deviation of the central atom increases up to Pd<sub>26</sub>. Pd<sub>26</sub> is a turning point for the central atom because the growing structure at this point has half filled equatorial sites in the Pd<sub>19</sub> cluster. There are visible maxima for these predicted magic sizes (Pd<sub>19</sub>, Pd<sub>23</sub>, Pd<sub>26</sub>, Pd<sub>29</sub>, Pd<sub>32</sub> and Pd<sub>34</sub>) in the minimum distance values.

For the 4-atom cluster, due to its regular pyramidal geometry, the maximum, minimum and mean pair distances of atoms (Figure 5b) are the same, 2.74 Å. The minimum pair distances decrease slightly while the mean pair distances increase with the increasing number of atoms. This is an expected behavior because the increase in the number of atoms leads to close packing of the clusters. When the number of atoms reaches 40, the minimum and mean values become 2.32 and 4.93 Å, respectively. However, the maximum pair distances have different trends in different size ranges. Structurally, different reorientations cause sudden increases and fluctuations in the maximum pair distances. For instance, from Pd<sub>4</sub> to Pd<sub>9</sub> all structures are in different orientations. From Pd<sub>9</sub> to Pd<sub>13</sub> the growing pattern based on pentagonal bipyramid structure results in a decrease of maximum pair distances. An addition of an atom to the triangular open sites of Pd<sub>13</sub> again leads to a new increase in the maximum pair distance for Pd<sub>14</sub>. The transformation from Pd<sub>14</sub> to the spherical form of Pd<sub>15</sub> produces a fluctuation in the distance. After 15 atoms, it turns back to expected growing pattern based on 13-atom geometry. The distance between two polar atoms of Pd<sub>19</sub> is the source of the rapid increase in the maximum pair distance from Pd<sub>18</sub> to Pd<sub>19</sub>. From Pd<sub>19</sub> to Pd<sub>26</sub> a slight decrease is observed in the maximum pair distances. For the par-

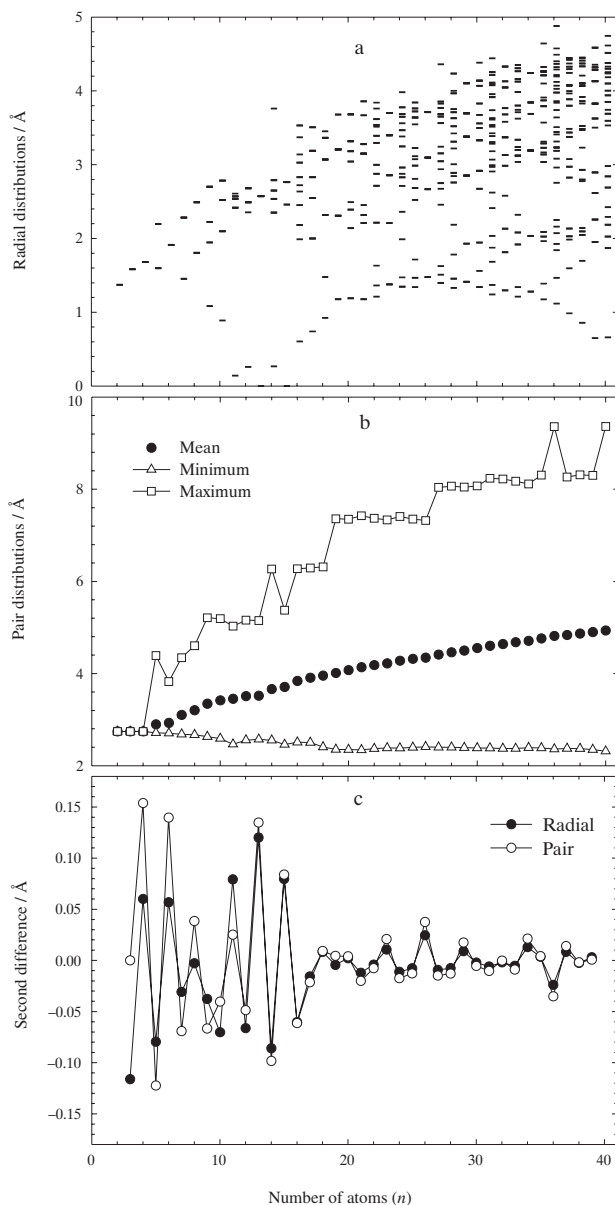


Figure 5. Displacement analysis of optimized structures for Pd<sub>2</sub>–Pd<sub>40</sub>; a) Radial distributions of atoms from center of the clusters, b) Pair distances of atoms in the clusters and c) Second finite difference of average values of distances of atomic pairs and from center of mass of the clusters.

ticular case of Pd<sub>26</sub> there is an interesting symmetry-like structure, crossing shape of the two 19-atom clusters. After passing the Pd<sub>26</sub> structure, there is a rapid increase in the maximum pair distance due to a new nonsymmetrical form of Pd<sub>27</sub>. There are also slight decreases in regions 27 to 30 and 31 to 34. Generally, any typical changes are determined around the magic sizes.

The second finite difference of the displacements of optimized structures for Pd<sub>2</sub>–Pd<sub>40</sub> are presented in Figure 5c for average values of distances of atomic pairs and from center of mass of the clusters as a function of cluster size. Structural reorientations of Pd<sub>4</sub>, Pd<sub>6</sub>, Pd<sub>8</sub> and Pd<sub>11</sub> lead to peaks in the values of the second finite

differences. Pd<sub>13</sub> and Pd<sub>15</sub> have peaks due to the effects of their spherical structures. In all cases, these two clusters have the same characteristics of the stability functions for both maximum and minimum displacements. As shown in the graph there are peaks visualizing all magic-like sizes, with only an exception observed for Pd<sub>19</sub>. These peaks for 23-, 26-, 29-, 34- and 37-atom clusters are related to their structures and their close packing sequences. They describe the reactive sites filled structures.

To investigate the growth mechanism in more detail, the density coefficients for number of atoms per volume of the clusters were also calculated. For each cluster, one can write

$$\sigma(n) = \frac{n}{r_n^3} \quad (9)$$

that defines the proportionality relation for the cluster density,<sup>45</sup> where  $n$  is the number of atoms and  $r_n$  is the radius of the cluster corresponding to the largest value of the radial distributions in Figure 5a. The stability function of the determined coefficients is

$$\Delta_2 \sigma = \sigma(n+1) + \sigma(n-1) - 2\sigma(n). \quad (10)$$

Figures 6a and 6b illustrate the density coefficients and their stability functions. As can be observed, there are large fluctuations in microcluster region with espe-

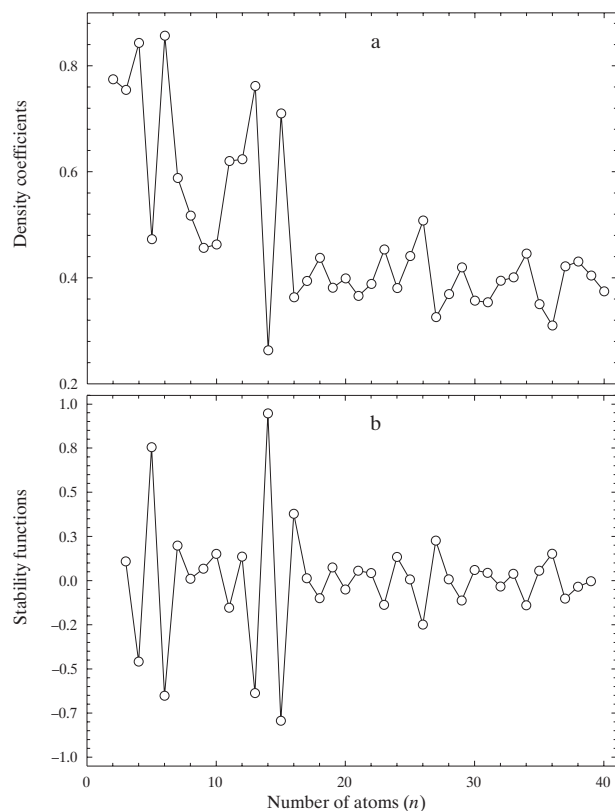


Figure 6. a) Density coefficients and b) their stability values through second finite differences.

cial attention near the region of the first magic number,  $n = 13$ . It means that they are reoriented through the changing of the atomic positions. This fluctuation is smaller for medium size clusters mainly because for larger clusters the orientation of the new clusters after rearrangement collision occurs on the surface atoms of the clusters. Moreover, adding new atoms for larger systems produces small fluctuations in the energy of the whole system as can be observed in Figure 3. The relaxation process is therefore less expensive and allows small rearrangement of the new cluster formation. Inner structures of these clusters generally keep their previous geometries unless the new atom added produces instability to the primitive cluster. The minima in the stability functions (Figure 6b) indicate that the relatively more symmetrical close packing size structures are 4, 6, 13, 15, 23, 26, 29, 34 and 37.

As discussed in Ref. 51, the analysis of the eigenvalues of the matrices that contain the moment of inertia (MoI) can provide insights to the geometry of the cluster. Therefore, MoI for these particular palladium clusters is analyzed in a similar way as that in Ref. 51 and the results are presented in Figure 7. The values ( $I_x$ ,  $I_y$  and  $I_z$ ) of MoI with respect to the three components of the Cartesian coordinates are plotted as functions of the cluster size in Figure 7a. The equation to calculate MoI is as follows

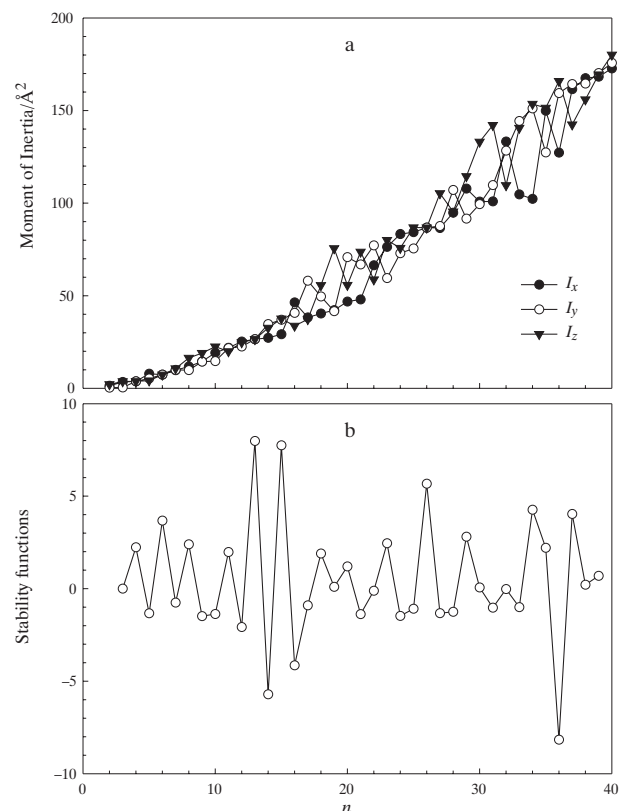


Figure 7. a) Moment of inertia for determined clusters and b) the stability values.

$$I_q = m \sum_{i=1}^n q_i^2, \quad q = x, y, z. \quad (11)$$

They have been calculated *via* assuming the mass of the particles as normalized to unit mass 1. The equal values of three MoI show that the cluster has a spherical structure. As observed from Figure 7 the sizes  $n = 4, 6, 13$  and  $26$  are obviously spherical geometries. The total MoI values and its second finite differences are

$$I_r = m \sum_{i=1}^n r_i^2, \quad r_i^2 = x_i^2 + y_i^2 + z_i^2 \quad (12)$$

$$\Delta_2 I_r = I_{r(n+1)} + I_{r(n-1)} - 2I_{r(n)}. \quad (13)$$

It is given in the stability graphs in Figure 7b. The maxima in this figure demonstrate that the relatively more spherical palladium structures have atoms sizes of 13, 15, 23, 26, 29, 34 and 47. Finally, the mean values ( $\bar{I}$ ) of the component dependent differences of MoI have been calculated by using absolute values of  $I_x - I_y$ ,  $I_y - I_z$  and  $I_z - I_x$  differences, which is

$$\bar{I} = \frac{|I_x - I_y| + |I_x - I_z| + |I_y - I_z|}{3}. \quad (14)$$

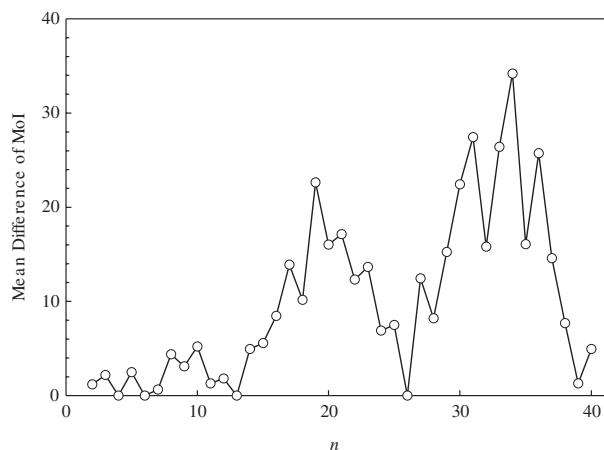


Figure 8. Mean value of componental difference of moment of inertia for the found clusters.

As presented in Figure 8 Pd<sub>4</sub>, Pd<sub>6</sub>, Pd<sub>13</sub> and Pd<sub>26</sub> are exactly in spherical symmetric geometries.

## CONCLUDING REMARKS

The primary dynamics of the Pd+Pd<sub>n-1</sub>→Pd<sub>n</sub> collision process described by a LJ type potential have been investigated in details by means of classical MD analysis. Palladium clusters were taken as a prototype and it was possible to show that the small clusters can realisti-

cally be used as a model for understanding the growing mechanisms for larger systems even though using a very qualitative potential energy function parameterized for crystal analysis. These studies produced a comprehensive analysis of dominant effects on cluster growing phenomena although the potential energy model used is not realistic. In addition, there was no possible investigations of the cluster energetics for this empirical potential since the results are not even qualitative. Therefore, this work suggests that new fitting potentials need to be evaluated for better understanding the real global minimum with emphasis to palladium clusters.

Finally, it is demonstrated that any palladium cluster can be obtained through the rearrangement collision as a tool in generating the possible candidates for the ground state and higher energy structures of palladium clusters. Moreover, the correspondence of the determined structures to magic numbers is in fair agreement with several recent reported studies<sup>41,45</sup> and shows that trends in the physical properties can be studied through the structural analysis of palladium clusters in the medium size range *via* these LJ-type geometries. The PEF used here may also be developed by adding any many-body terms for future studies of atomic clusters.

*Acknowledgements.* – This work was supported by CNPq and FAPEMIG in Brazil and by Research Fund of Erciyes University (Project Number: FBA.06.07) in Turkey. One of the authors (MB) would like to thank the Brazilian Research Agency (CNPq) for a postdoctoral research grant. We would also like to thank the unknown referees for their constructive comments. We would also like to thank Professor James Lewis Wardell and Selver Uslu that contribute to our final version of the manuscript.

## REFERENCES

1. E. R. Bernstein (Ed.), *Atomic and Molecular Clusters*, Elsevier, Amsterdam, 1990.
2. H. Haberland (Ed.), *Clusters of Atoms and Molecules*, Springer, Berlin, 1994.
3. T. P. Martin, *Large Clusters of Atoms and Molecules*, Springer, Dordrecht, 1996.
4. R. L. Johnston, *Atomic and Molecular Clusters*, Taylor and Francis, London, 2002.
5. P. Jena, S. N. Khanna, and B. K. Rao (Eds.), *Physics and Chemistry of Finite Systems: From Clusters to Crystals*, Kluwer Academic, Dordrecht, 1992.
6. M. Büyükat, E. Borges, J. C. Belchior, and J. P. Braga, *Can. J. Chem.* **85** (2007) 47–55.
7. M. Büyükat, Z. B. Güvenç, S. Özçelik, P. Durmuş, and J. Jellinek, *Int. J. Mod. Phys. C* **16** (2005) 295–308.
8. M. Büyükat and Z. B. Güvenç, *Braz. J. Phys.* **36** (2006) 720–724.
9. M. Büyükat, M. Karabacak, S. Özçelik, Z. B. Güvenç, and J. Jellinek, *Bulgarian J. Phys.* **27** (2000) 110–114.
10. E. Kurt, M. Büyükat, and Z. B. Güvenç, *Phys. Scr.* **74** (2006) 353–316.

11. H. B. Wu, S. R. Desai, and L. S. Wang, *Phys. Rev. Lett.* **76** (1996) 212–215.
12. L. S. Wang, X. Li, and H. F. Zhang, *Chem. Phys.* **262** (2000) 53–63.
13. S. R. Liu, H. J. Zhai, and L. S. Wang, *Phys. Rev. B* **64** (2001) 153402.
14. S. R. Liu, H. J. Zhai, and L. S. Wang, *J. Chem. Phys.* **117** (2002) 9758–9765.
15. S. R. Liu, H. J. Zhai, M. Castro, and L. S. Wang, *J. Chem. Phys.* **118** (2003) 2108–2115.
16. I. M. L. Billas, A. Châtelain, and W. A. de Heer, *J. Magn. Magn. Mater.* **168** (1997) 64–84.
17. O. Diéguez, M. M. G. Alemany, C. Rey, P. Ordejón, and L. J. Gallego, *Phys. Rev. B* **63** (2001) 205407.
18. P. Bobadova-Parvanova, K. A. Jackson, S. Srinivas, M. Hori, C. Köhler, and G. Seifert, *J. Chem. Phys.* **116** (2002) 3576–3587.
19. C. Köhler, G. Seifert, and T. Frauenheim, *Chem. Phys.* **309** (2005) 23–31.
20. J. L. Simonds, *Phys. Today* **48** (1995) 26–32.
21. J. A. Alonso, *Chem. Rev.* **100** (2000) 637–677.
22. C. Brechignac, P. Cahuzac, F. Carlier, M. de Frutos, and J. Leygnier, *J. Chem. Soc., Faraday Trans.* **86** (1990) 2525.
23. M. Karabacak, S. Özçelik, and Z. B. Güvenç, *Surf. Sci.* **507** (2002) 636–642.
24. M. Karabacak, S. Özçelik, and Z. B. Güvenç, *Surf. Sci.* **532** (2003) 306–311.
25. S. Y. Wang, J. Z. Yu, H. Mizuseki, J. A. Yan, Y. Kawazoe, and C. Y. Wang *J. Chem. Phys.* **120** (2004) 8463–8468.
26. A. Sebetçi and Z. B. Güvenç, *Modelling Simul. Mater. Sci. Eng.* **13** (2005) 683–698.
27. W. Kohn and L. P. Sham, *Phys. Rev. A* **140** (1965) 1133.
28. H. Arslan, *Int. J. Mod. Phys. C* **18** (2007) 1351–1359.
29. M. Büyükatata, *J. Theo. Comp. Chem.* **6** (2007) 81–97.
30. M. Büyükatata and J. C. Belchior, *J. Braz. Chem. Soc.* (2008) in press.
31. J. M. Penisson and A. Renou, *J. Cryst. Growth* **102** (1990) 585–591.
32. M. Josè-Yacamàn, M. Marin-Almazo, and J. A. Ascencio, *J. Mol. Catal. A* **173** (2001) 61–74.
33. I. Efremenko, *J. Mol. Catal. A* **173** (2001) 19–59.
34. P. Nava, M. Sierka, and R. Ahlrichs, *Phys. Chem. Chem. Phys.* **5** (2003) 3372–3381.
35. S. Krüger, S. Vent, F. Nörtemann, M. Staufer, and N. Rösch, *J. Chem. Phys.* **115** (2001) 2082–2087.
36. M. Moseler, H. Häkkinen, R. N. Barnett, and U. Landman, *Phys. Rev. Lett.* **86** (2001) 2545–2548.
37. G. Rossi, C. Mottet, F. Nina, and R. Ferrando, *J. Phys. Chem. B* **110** (2006) 7436–7422.
38. C. Massen, T. V. Mortimer-Jones, and R. L. Johnston, *J. Chem. Soc., Dalton Trans.* (2002) 4375–4388.
39. J. Rogan, R. Ramírez, A. H. Romero, and M. Kiwi, *Eur. Phys. J. D* **28** (2004) 219–228.
40. T. Mohri, T. Horiuchi, H. Uzawa, M. Ibaragi, M. Igarashi, and F. Abe, *J. Alloys Compd.* **317** (2001) 13–18.
41. M. Büyükatata, E. Borges, J. P. Braga, and J. C. Belchior, *J. Alloys Compd.* **403** (2005) 349–356.
42. In: NBS Technical Note, Selected Values of Chemical Thermodynamic Properties, 1969, p 270.
43. In: Selected Values of the Thermodynamic Properties of the Elements, ASM, 1973.
44. In: Landolt-Bornstein III/14-a, Structure Data of Elements and Intermetallic Phases, 1988.
45. M. Büyükatata, *Physica E* **33** (2006) 182–190.
46. D. J. Wales and J. P. K. Doye, *J. Phys. Chem. A* **101** (1997) 5111–5116.
47. Z. El-Bayyari, H. Oymak, and H. Kökten, *Int. J. Mod. Phys. C* **18** (2004) 917–930.
48. M. Mavrikakis, P. Stoltze, and J. K. Nørskov, *Catal. Lett.* **64** (2000) 101–106.
49. N. S. Phala, G. Klatt, and E. van Steen, *Chem. Phys. Lett.* **395** (2004) 33–37.
50. G. Scoles (Ed.), *The Chemical Physics of Atomic and Molecular Clusters*, North-Holland, Amsterdam, 1990.
51. V. G. Grigoryan and M. Springborg, *Chem. Phys. Lett.* **375** (2003) 219–226.
52. J. Uppenbrink and D. J. Wales, *J. Chem. Phys.* **96** (1992) 8520–8534.
53. J. Jortner, *Z. Phys. D* **24** (1992) 247–275.
54. R. A. Lordeiro, F. F. Guimaraes, J. C. Belchior, and R. L. Johnston, *Int. J. Quantum Chem.* **95** (2003) 112–115.
55. Ş. Erkoç, *Physica E* **8** (2000) 210–218.

## SAŽETAK

### Studija grozdova paladija molekulskom dinamikom: Analiza strukturnih stabilnosti i energija Pd<sub>n</sub> (n ≤ 40) u ovisnosti o veličini korištenjem potencijala Lennard-Jonesovog tipa

Mustafa Büyükatata i Jadson C. Belchior

Moguće stabilne strukture i energije grozdova paladija Pd<sub>n</sub> (n = 2–40) su istražene provođenjem simulacija molekulske dinamike zasnovanima na Lennard-Jonesovom potencijalu. Kako bi se odredilo preferirani mehanizam rasta, obrazac rasta Pd<sub>n</sub> grozdova je analiziran pomoću sudarnih pregradnji i tehnika gašenja. Nađeno je da grozdovi paladija preferiraju trodimenzionalne strukture te da kuglasti grozdovi srednjih veličina čini se da posjeduju os petog reda. Nalazi su uspoređeni s ranijim teorijskim studijama.